Hindawi Publishing Corporation
International Journal of Antennas and Propagation
Volume 2016, Article ID 2829357, 14 pages
http://dx.doi.org/10.1155/2016/2829357

Research Article

A Compact Novel Three-Port Integrated Wide and Narrow Band Antennas System for Cognitive Radio Applications

N. Anvesh Kumar and A. S. Gandhi

Department of ECE, VNIT, Nagpur, India

Correspondence should be addressed to N. Anvesh Kumar; nellaanvesh@gmail.com

Received 24 June 2016; Revised 15 August 2016; Accepted 20 September 2016

Academic Editor: Renato Cicchetti

The design of a three-port radiating structure, integrating wide and narrow band antennas for cognitive radio applications, is presented. It consists of a UWB antenna for spectrum sensing and two narrow band antennas for wireless communication integrated on the same substrate. The UWB antenna covers the complete UWB spectrum (3.1 GHz to 10.6 GHz) approved by FCC. In the two narrow band antennas, each antenna presents dual bands. In particular, the first narrowband antenna resonates at 6.5 GHz, covering the frequency band between 6.36 GHz and 6.63 GHz, and at 9 GHz, covering the frequency band between 8.78 GHz and 9.23 GHz, presenting minimum return loss values of 28.3 dB at 6.5 GHz and 20.5 dB at 9 GHz, respectively. Similarly, the second one resonates at 7.5 GHz, covering the frequency band between 7.33 GHz and 7.7 GHz, and at 9.5 GHz, covering the frequency band between 9.23 GHz and 9.82 GHz, presenting minimum return loss values of 19.6 dB at 7.5 GHz and 28.8 dB at 9.5 GHz, respectively. Isolation among the three antennas is less than −20 dB over the UWB frequency spectrum. These antennas are realized on a FR4 substrate of dimensions 30 mm × 30 mm × 1.6 mm. Experimental results show a good agreement between the simulated and measured results.

1. Introduction

In today's wireless communication, because of the increasing growth of applications, there is a great demand for bandwidth. But, as for the requirements, the spectrum bandwidth cannot be increased beyond limits due to frequency and economic constraints. In licensed spectrum, many channels are free due to their inefficient utilization. So, these empty channels can be utilized to overcome the problem of limited spectrum. In 2002, FCC has proposed several solutions to enhance the licensed spectrum utilization efficiency. These solutions are divided into three categories, the spectrum leasing, the spectrum reallocation, and the spectrum sharing [1–4]. The spectrum sharing is also divided into three types. The first one is the open spectrum sharing, the second one is the hierarchical spectrum sharing, and the third one is the dynamic spectrum allocation. In the hierarchical spectrum sharing approach, we employ cognitive radio technology to utilize unused or free licensed channels. In this model, the licensed spectrum is assumed to be owned by the primary users, who do not fully utilize their channels. Hence, the secondary users utilize these free channels until the primary users demand them. In this case, the secondary users have to shift on to other free channels to maintain the continuous communication as shown in Figure 1(b). In cognitive radio applications, the radio environment is continuously monitored for spectrum holes. In this process, if any spectrum hole is identified, then that channel is used for other wireless communication applications. In general, UWB antennas are adopted for spectrum sensing while frequency reconfigurable narrow band (NB) antennas are employed for communication [5, 6]. In modern wireless and portable systems, conventional antennas are not compatible with these applications. Therefore, planar monopole antennas are highly preferred due to their advantages like small size, low cost, lightweight, easy integration with planar structures, and easy fabrication [7].

In recent years, dual port integrated UWB and frequency reconfigurable NB antenna systems are becoming very popular for cognitive radio applications. In these systems, the

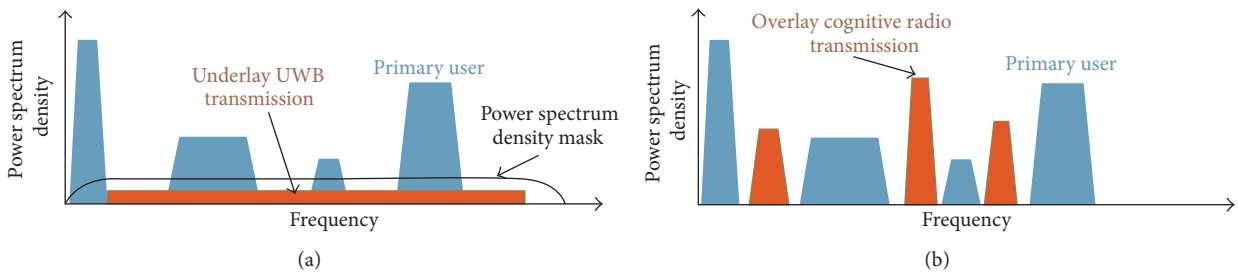

Figure 1: Hierarchal spectrum sharing approaches. (a) Spectrum underlay. (b) Spectrum overlay [1].

UWB antennas are used for spectrum sensing and the reconfigurable narrow band antennas are used for communication. In the NB antennas reconfiguration is introduced to support many communication frequencies by using a single antenna. We investigated numerous dual port integrated antenna structures presented in the literature [8–15]. An integrated UWB and rotatable NB antennas structure of dimensions 70 mm × 50 mm × 1.6 mm is reported in [8]. In this paper, the authors make use of a stepper motor controlled by a computer to switch between five different NB antennas printed on a circular substrate. These NB antennas are able to obtain single resonance in each case within 2 to 10 GHz frequency spectrum. In [9], the authors focused on an integrated wide-narrow band antenna structure of dimensions 68 mm × 54 mm × 0.79 mm for multistandard radio. In this structure, the reconfiguration is implemented by introducing three different resonant matching circuits. In each case, the NB antennas are able to yield one resonating band within 4 to 10 GHz frequency spectrum. An integrated dual port UWB and reconfigurable NB antennas structure of dimensions 50 mm × 50 mm × 1.6 mm is discussed in [11]. In this design, the reconfiguration is performed by employing three switches on the NB antenna to achieve eight resonating bands in four cases within 3 to 10 GHz frequency spectrum. In [12], the authors presented an integrated UWB and optically controlled reconfigurable NB antennas structure having dimensions 50 mm × 45.5 mm × 1.6 mm. In this structure, the NB antenna is reconfigured by pumping a laser light on to the two silicon switches to attain three resonating bands within 3 to 6 GHz frequency spectrum.

However, the discussed reconfigurable mechanisms have some drawbacks, like the negative effect of biasing lines used to control switches states, the power consumption, the nonlinearity effects of switches, and the slow tuning. Moreover, sometimes they require additional biasing circuitry or motors to achieve antenna reconfigurability [4, 16]. In cognitive radio applications, the main purposes of employing the reconfigurable antennas are to reduce cost and space and for fast tuning. But all these reconfigurable mechanisms make the printed antennas bulky and complex, which nullify all the advantages of planar antennas. Even these reconfigurable mechanisms are very difficult to implement in practice. So, to overcome these drawbacks and maintain all the advantages of planar antennas, we propose an integrated three-port planar antennas design. Among these three ports, a UWB antenna that is accessible at the first port is used for spectrum sensing and the two NB antennas, which are accessible at the remaining two ports, are used for communication. Here also reconfiguration may be performed between the two NB antennas such that only one NB antenna is operated at a time. The selection of a particular narrow band antenna depends on the sensed hole in the frequency spectrum to which it is matched. The main challenges in these designs are isolation and space reduction.

In this paper, a three-port antenna system for cognitive radio applications is presented. The radiating system is composed of a UWB antenna for spectrum sensing and two narrow band antennas for wireless communications. The antennas are printed on a low cost FR4 substrate having dimensions 30 mm × 30 mm × 1.6 mm. The analysis and design of the proposed antenna system were performed using the full-wave commercial software HFSS 14.0 based on the finite element method (FEM). The paper is organized into 4 sections. In Section 2, the design of a simple and small size planar monopole UWB antenna is illustrated. In Section 3, the analysis, design, and results of the proposed three-port antenna system is presented and finally in Section 4 some concluding remarks are provided. Details of the proposed antenna are given in the next sections.

2. Proposed Single Port UWB Antenna Design

In this section, the preliminary design of a one-port UWB antenna is presented. This design takes into account the scientific results available in the literature [17–23]. These results show that round shapes, round edges, partial grounds, and partial grounds with specially designed slots play a major role in obtaining UWB performance [6, 18, 19]. So, on the basis of these observations, a circular monopole with a partial ground as shown in Figure 2 was chosen as a radiating element.

For this antenna design, the equation proposed in [23] is used to find out its geometrical parameters. By using this equation

$$f_L = \frac{7.2\,\text{GHz}}{\{(L + r + p) \times k\}}, \tag{1}$$

where f_L is selected lower band edge of the UWB frequency spectrum ($f_L = 3$ GHz), p (feed gap) = 0.14 cm, $L = 2 * a$ and

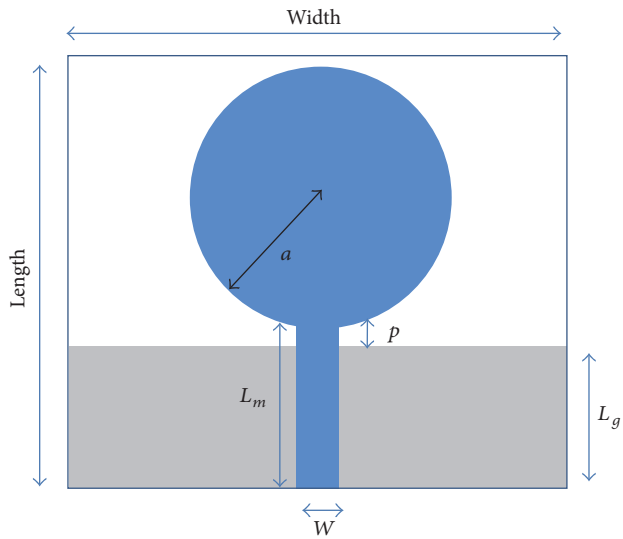

Figure 2: Geometry of a circular planar monopole UWB antenna. The main geometrical parameters are indicated in the figure.

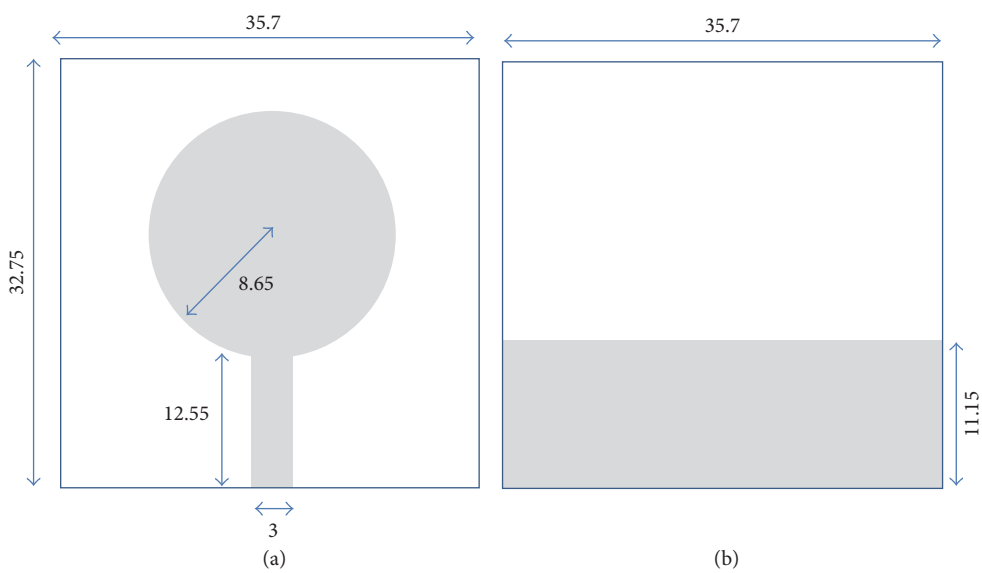

Figure 3: The circular planar monopole UWB antenna geometry. (a) Top view. (b) Bottom view [all dimensions are in mm].

$r = a/4$, and $k = 1.15$ (constant), it is possible to evaluate radius (a) of monopole suitable to ensure the input in-band to the frequency f_L, with an accuracy of about 10%. Using (1) the radius (a) is found to be 8.65 mm. Then, the substrate size was optimized so as to obtain an impedance bandwidth with VSWR ≤ 2 in the UWB frequency band (from 3.1 GHz up to 10.6 GHz). After completing the optimization process a substrate having dimensions 32.75 mm $\times$ 35.7 mm has been found. The geometry of the UWB monopole antenna, including the optimized geometrical parameters, is reported in Figure 3.

For a proper impedance matching over the complete UWB spectrum, a microstrip line of 12.55 mm $\times$ 3 mm size was selected. The return loss performance of the discussed antenna design can be inferred from Figure 4. The resulting monopole antenna covers a frequency band from 2.62 GHz up to 11.15 GHz with VSWR ≤ 2, thus including the complete UWB spectrum (from 3.1 GHz to 10.6 GHz) approved by FCC in 2002 [24]. However, the proposed antenna's return loss performance is poor, while the dielectric substrate and the partial ground dimensions are larger than the active patch (see Figure 3). Therefore, to reduce the antenna dimensions and to achieve better UWB performances, we modified the proposed antenna in a systematic way. Initially, the substrate dimensions are reduced to 30 mm $\times$ 19 mm. These dimensions cannot be reduced further because the active

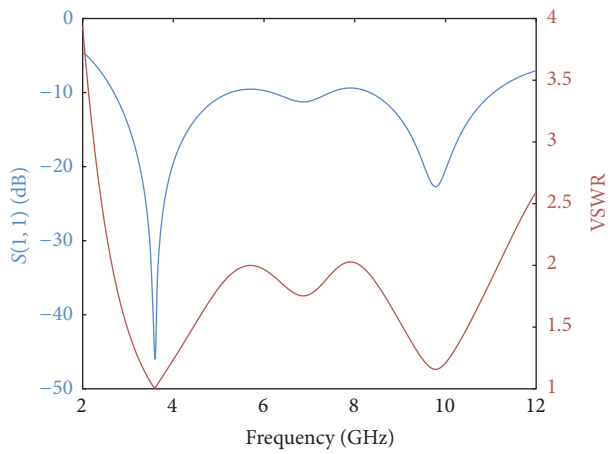

Figure 4: Frequency behavior of the UWB monopole antenna input reflection coefficient.

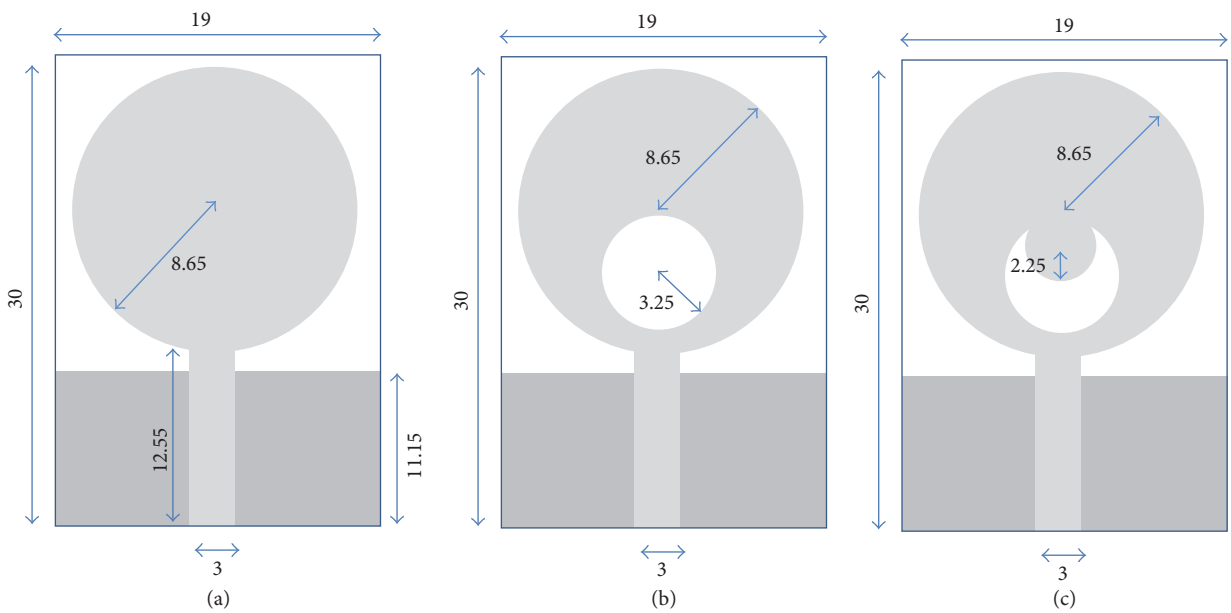

Figure 5: Design steps adopted to realize the UWB monopole antenna: (a) first step, (b) second step, and (c) third step.

patch almost exists on the entire substrate as shown in Figure 5(a). Then, a step-by-step optimization process, as shown in Figures 5(a), 5(b), 5(c), and 7, to obtain better UWB performances has been employed. To do this, one circular slot and one circular fill in the top layer and a circular slot on the bottom layer are introduced (see Figure 7(b)). The geometry, the dimensions, and positions of these shapes are carefully optimized using the adopted full-wave software.

Round shapes and round edges have been employed because, as pointed out earlier, they yield better UWB performances. These aspects can be appreciated by looking at the frequency behavior of the return loss of the three design solutions described above (see Figure 6). Return loss performances of the three-step design are shown in Figure 6. Even though the realization of suitable shaped slots in the metal patch is able to increase the antenna bandwidth, it prevents covering the entire UWB band as it appears in Figure 6. Therefore, an optimized circular slot of 1.75 mm is realized on the upper edge of the ground plane in order to improve the performance of the return loss (see Figure 7(b)). This slot allows for obtaining the desired antenna impedance matching in the UWB band as shown in Figure 8. Return loss performance of the optimized UWB monopole antenna is shown in Figure 8.

As it appears from Figure 8, the etched shapes realized on the top and bottom layers have a significant impact on achieving a UWB spectrum ranging from 2.62 GHz to 12.63 GHz. From the simulated result it is obvious that the proposed UWB antenna is suitable to cover the complete UWB spectrum. Because of small size and better performance, the proposed UWB antenna can be used in many UWB wireless communication applications.

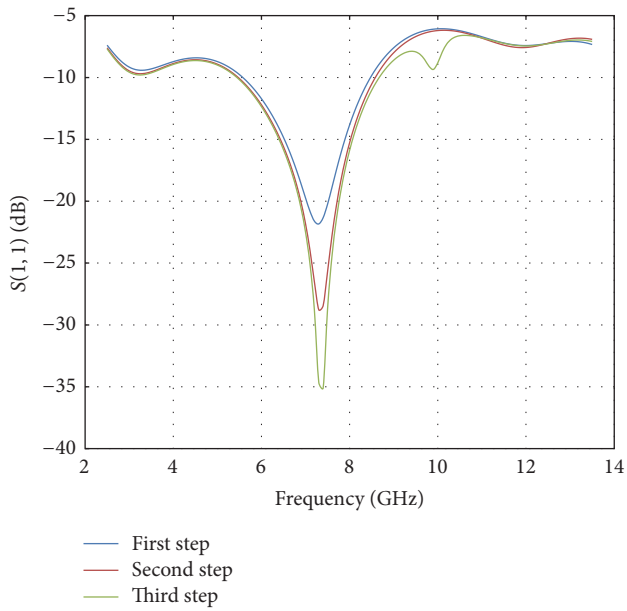

Figure 6: Antenna input reflection coefficient versus frequency. The curves refer to the first three steps' design.

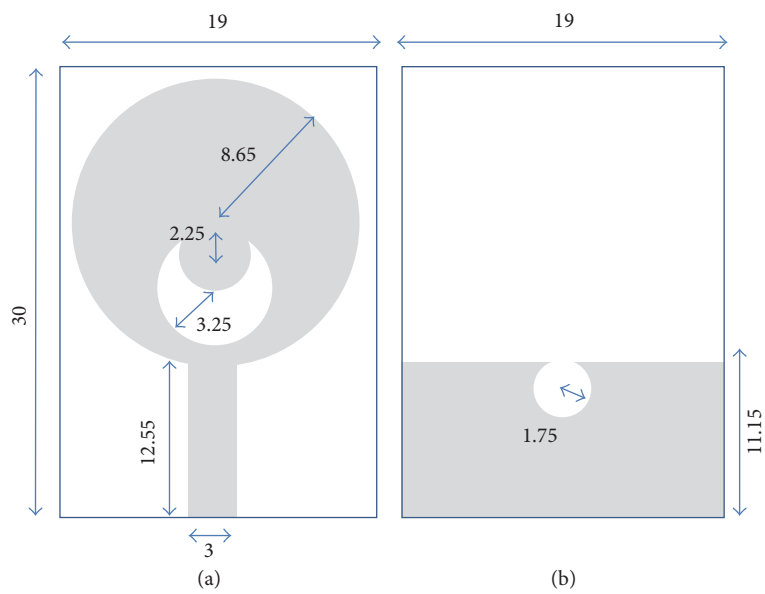

Figure 7: The final UWB antenna geometry. (a) Top view. (b) Bottom view.

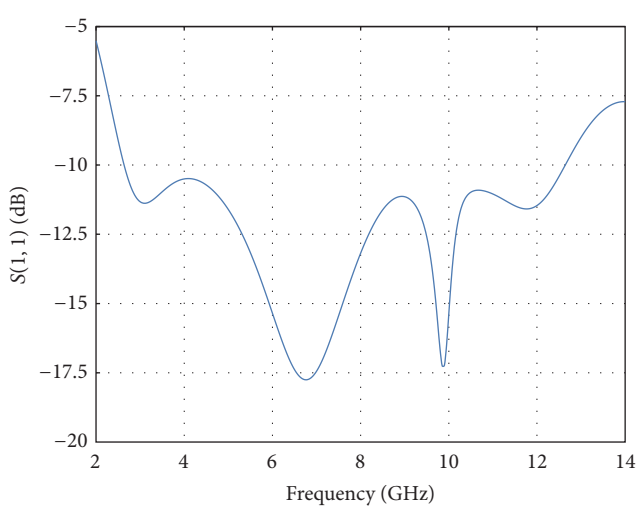

Figure 8: Antenna input reflection coefficient versus frequency of the final version of the UWB antenna.

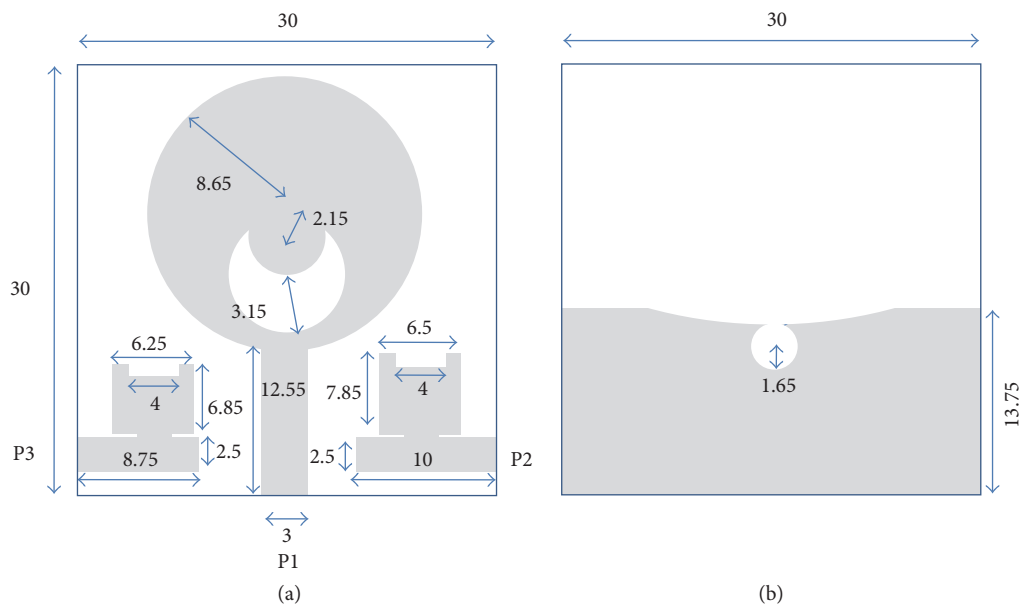

Figure 9: Proposed integrated UWB and NB antennas geometry. (a) Top view. (b) Bottom view.

3. Analysis and Design of the Three-Port Radiating Structure

In this section, we discuss the proposed three-port antenna system composed of a UWB and two NB antennas integrated on the same substrate. As discussed earlier, each antenna has an independent excitation port as shown in Figure 9(a). Therefore, to achieve good isolation characteristics between each antenna, the substrate dimensions, the active patch, and the ground plane structures are carefully modified. In particular, a UWB antenna linked with the first port is used for spectrum sensing, while the remaining two NB antennas linked with the other two ports of the antenna system are used for wireless communications. The UWB and the two NB antennas are printed on top surface of FR4 dielectric substrate in such a way that electromagnetic isolation among them is very high. In general, for UWB antennas partial grounds are highly preferred, while for narrow band antennas full grounds are widely used. Here also the bottom layer shown in Figure 9(b) is acting as a partial ground for the UWB antenna and as a full ground for the two narrow band antennas. In the proposed design, we incorporated various slots on the top and bottom layers to enhance return loss performance. Top and bottom views of the proposed three-port antenna system are shown in Figure 9.

In particular, the monopole of the UWB antenna has been further optimized (see Figure 10(b)) with respect to the initial design discussed in the previous section (see Figure 10(a)), while a chamfer has been introduced in the upper part of the ground plane, as shown in Figure 9(b), to enhance the UWB antenna performance.

After completing the design of the UWB antenna the analysis and design of two narrow band antennas forming the proposed antenna system are presented. In the proposed design, each of the two NB antennas has been designed so as to achieve a dual-band behavior useful for various wireless applications. To obtain this behavior on each rectangular patch antenna a slot has been realized, while a stub has been introduced along its feeding microstrip line (see Figure 9(a)). In particular, the slot realized on the rectangular patch controls the upper resonant band, while the stub inserted along the microstrip line allows for controlling the lower resonant band. The rectangular slot realized in the patch allows for increasing the electrical length enabling a shift of the upper resonant band toward lower frequencies. Note that the usual mathematical relationships between the length and the width, useful to design of rectangular patch antennas, are no longer applicable because of the irregular shapes, the small size, and the mutual coupling effects between the three antennas forming the radiating system. Furthermore, the small size of the realized NB antennas allows for obtaining a high electrical insulation. Top and bottom views of the prototype of the proposed antenna system are shown in Figure 11.

In the cognitive radio applications, during the operation of the proposed antenna system, the UWB antenna and one of the two NB antennas are operated for sensing and communication, while the other NB antenna is on standby. The selection of the particular NB antenna depends on the sensed hole in the frequency spectrum to which it is matched. This makes two possible different operative conditions. In the first condition the UWB antenna and the first NB antenna are operative, whereas in the second case the UWB antenna and the second NB antenna are active. This means that in the first case the antennas connected to Port 1 and Port 2 are excited, while the antenna connected to Port 3 is closed on a 50 Ω matched load. Similarly, in the second case the antennas connected to Port 1 and Port 3 will be excited, while the antenna connected to Port 2 will be closed on a matched

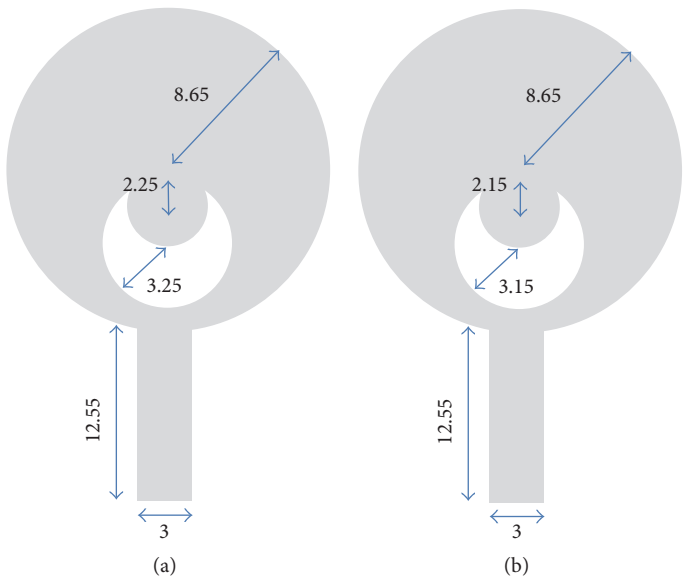

Figure 10: Geometry of the UWB antenna. (a) Preliminary design and (b) final design.

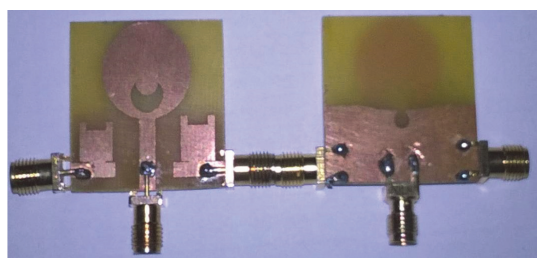

Figure 11: Top and bottom views of the fabricated prototype.

load. These two operative situations have been tested using a vector network analyzer (VNA).

3.1. Performance of the Radiating System in the First Operative Condition. The performances of the radiating system in the first operative condition, namely, with Ports 1 and 2 excited and with Port 3 closed on matched load, are derived by the analysis of the frequency behavior of the scattering parameters, of the gains, and of the radiation patterns of the three-port network forming the antenna system. In particular, by analyzing the frequency behavior of the parameter S_{11}, depicted in Figure 12, it results that the UWB antenna covers the frequency band ranging between 2.76 GHz and 13.96 GHz, with an increasing gain which varies between about 0.54 dBi and 5.58 dBi (see Figure 13) and with E- and H-radiation patterns described by the curves reported in Figure 14.

Different is the radiative behavior of the first NB antenna which resonates at 6.5 GHz and 9 GHz (see Figure 15) with return loss values of 28.3 dB at 6.5 GHz and 20.5 dB at 9 GHz, respectively. As it appears from Figure 15 the antenna exhibits a dual-band behavior covering the frequency bands between

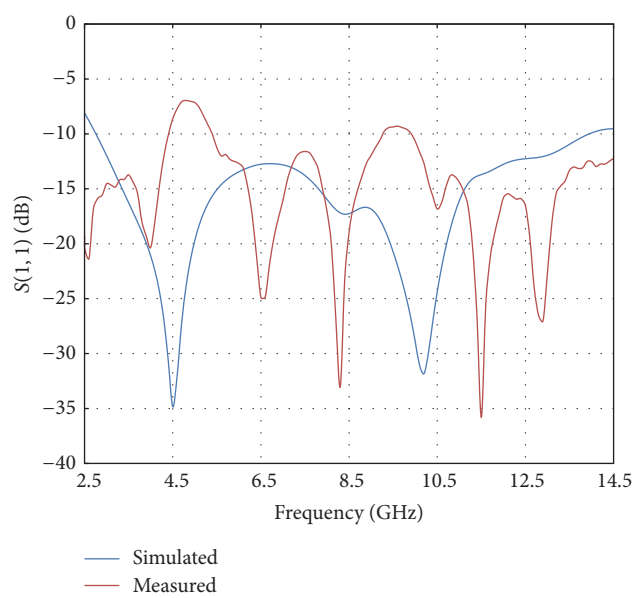

Figure 12: Comparison of simulated and measured reflection coefficients of the UWB antenna.

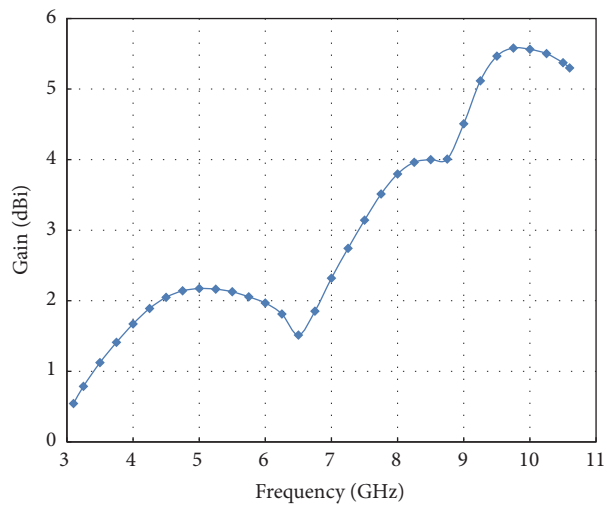

Figure 13: Peak gains versus frequencies plot of the UWB antenna.

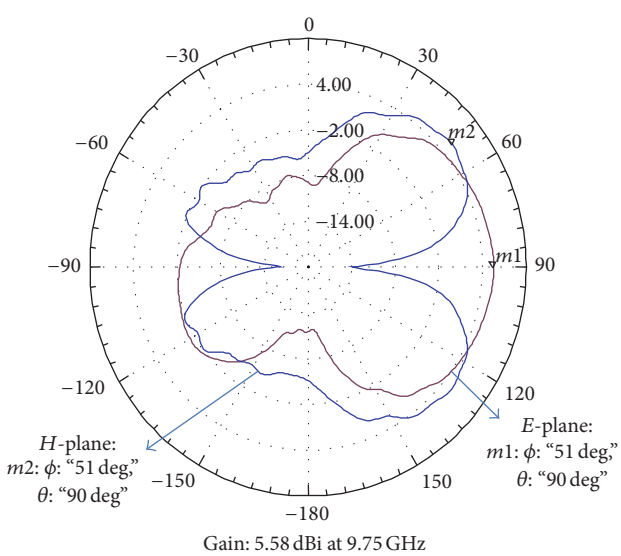

Figure 14: 2D radiation pattern of the UWB antenna at 9.75 GHz.

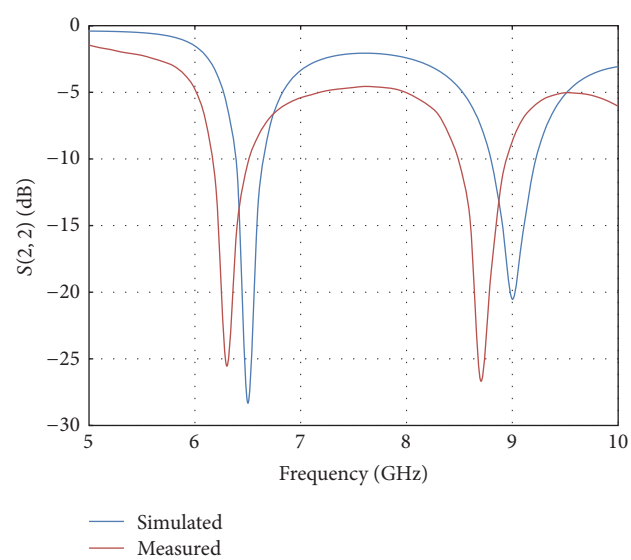

Figure 15: Comparison of simulated and measured reflection coefficients of the first NB antenna.

6.36 GHz and 6.63 GHz and between 8.78 GHz and 9.23 GHz, respectively. As discussed earlier, the slot in the rectangular patch is employed to generate the upper resonant band, while the stub added to the microstrip line is used to achieve the lower resonant band. To better understand the role of these shapes, the computed surface current distributions, excited on the first proposed NB antenna at the frequencies of 6.5 GHz and 9 GHz, are shown in Figure 16.

As it can be observed from Figure 16, the strong surface currents are distributed along the edges of microstrip line stub at 6.5 GHz and along the edges of slot on the rectangular patch at 9 GHz. Thus it is clearly evident that the radiation in the 6.5 GHz band is due to microstrip line added with stub and the radiation in 9 GHz band is due to slotted rectangular patch. The radiation patterns in the E- and H-plane at the two mentioned resonant frequencies are shown in Figure 17.

From these diagrams it appears that the antenna exhibits gains of approximately 3.03 dBi and 2.53 dBi, respectively. The characteristics of the narrow band antenna discussed above were derived by means of an extensive parametric analysis obtained by varying the length of the slot and of the microstrip stub. In particular, as discussed before, the rectangular slot controls the higher frequency band, while the microstrip stub controls the lower one. In particular, Figure 18(a) shows the frequency behavior of the reflection coefficient of the first NB antenna when the slot length varies. As it can be seen the optimal size is obtained for a slot length

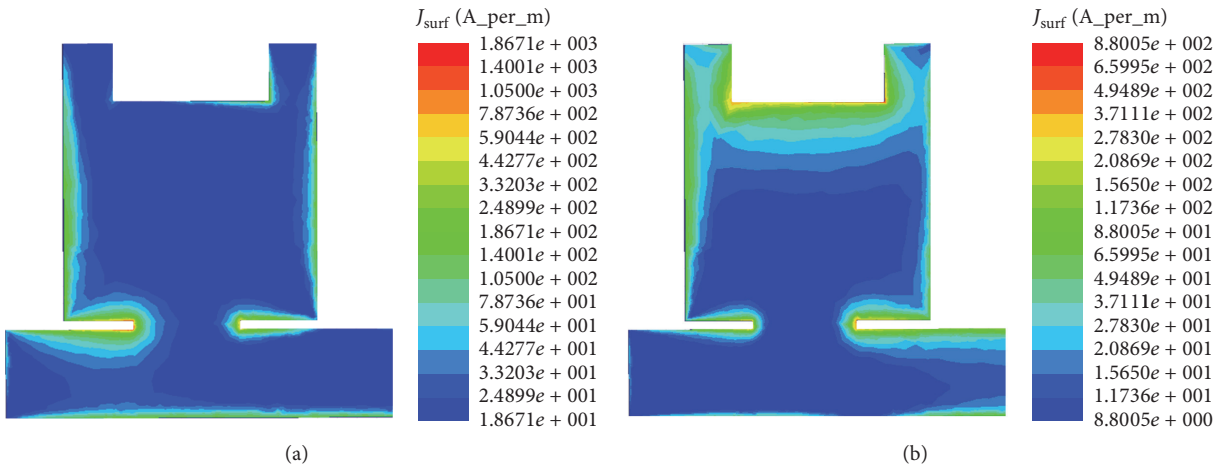

Figure 16: Simulated surface current distribution on the NB antenna at (a) 6.5 GHz and (b) 9 GHz.

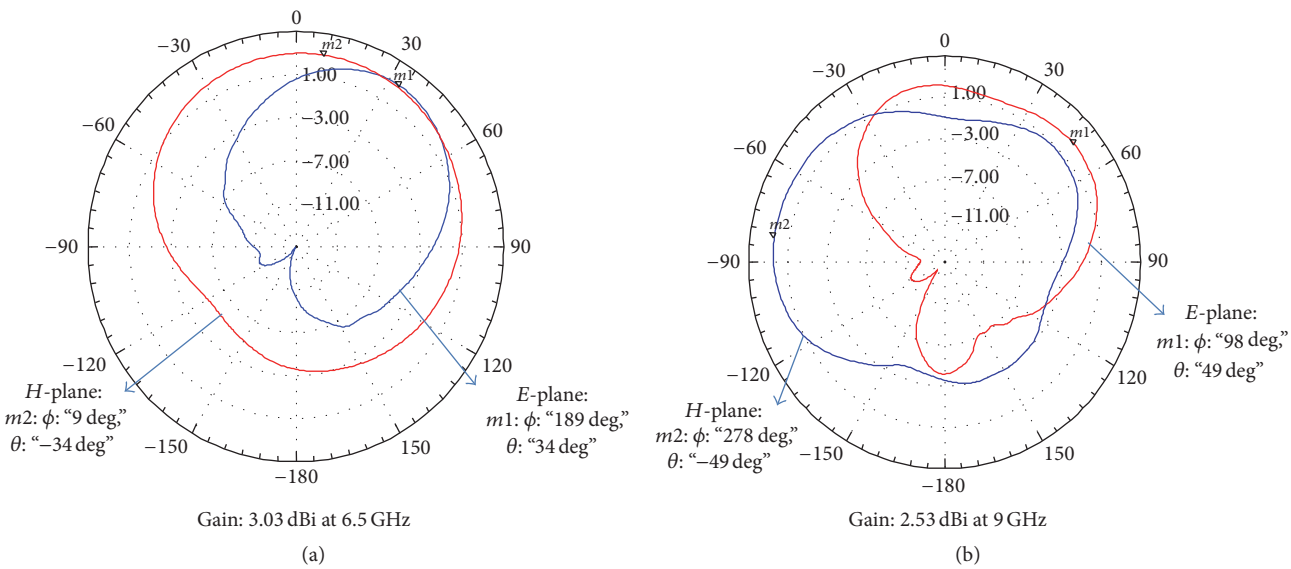

Figure 17: 2D radiation patterns of the NB antenna at (a) 6.5 GHz and (b) 9 GHz.

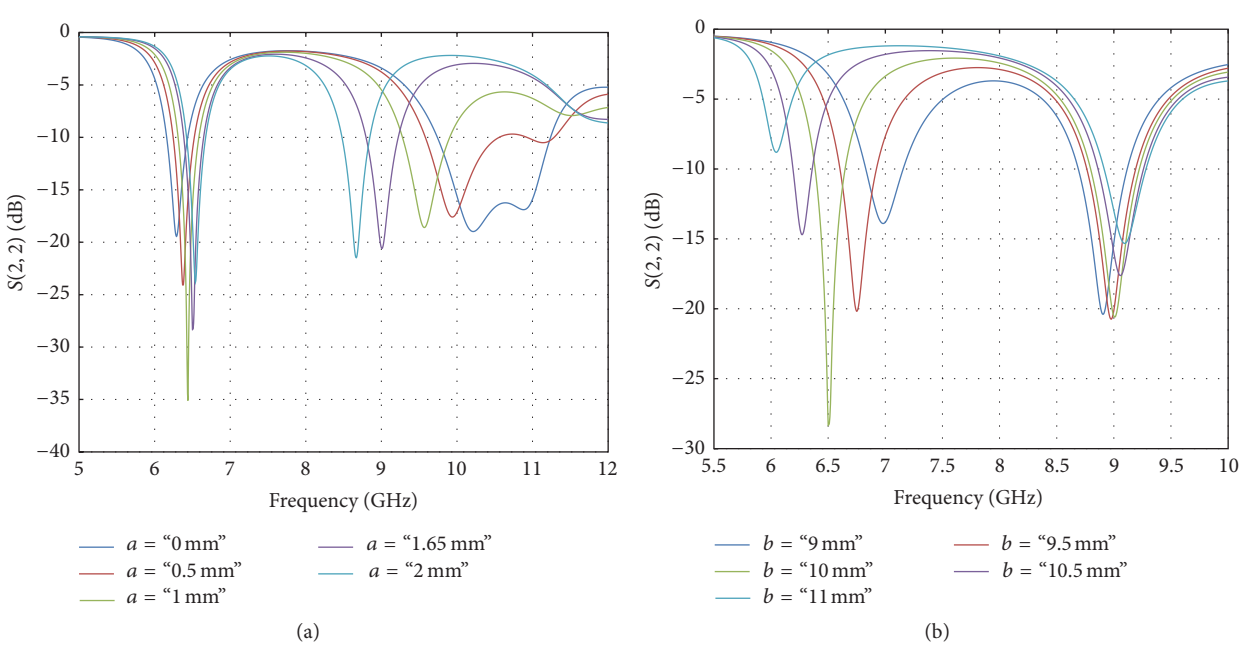

Figure 18: Reflection coefficients of the first NB antenna for (a) slot length variations and (b) microstrip stub length variations.

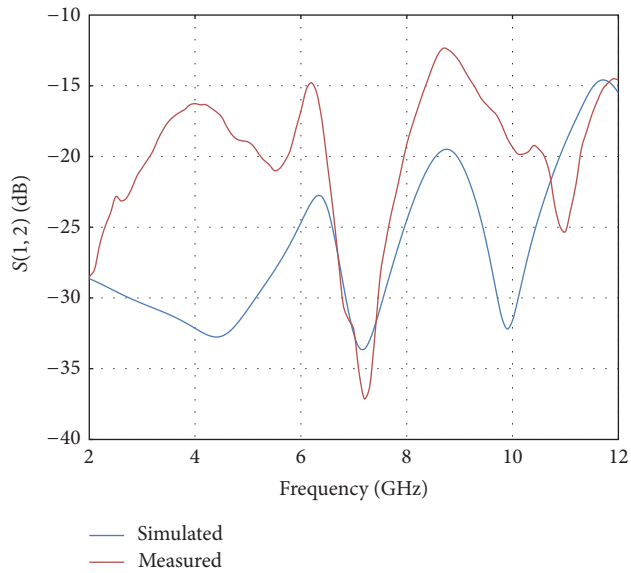

Figure 19: Comparison of simulated and measured transmission coefficients between the UWB and the first NB antenna ports.

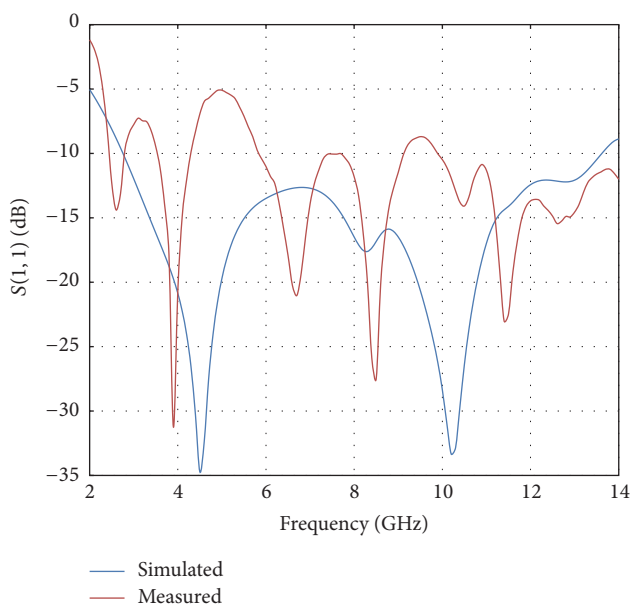

Figure 20: Comparison of simulated and measured reflection coefficients of the UWB antenna.

of 1.65 mm. Then the stub length, useful for tuning the lower frequency band, has been varied. From Figure 18(b) it appears that the optimized value of its length is 10 mm.

Finally, the frequency behavior of the scattering parameter S_{12}, depicted in Figure 19, shows that the electrical insulation with the UWB antenna is kept below −20 dB.

3.2. Performance of the Radiating System in the Second Operative Condition. After analyzing the behavior of the antenna system in the first operative condition, the behavior of the same, in the second operative condition, is considered. This last situation refers to the UWB antenna excited at Port 1 with the second NB antenna excited at Port 3 and with the first NB antenna closed on a matched load. Also in this case the UWB antenna covers the UWB band. In fact, as shown in Figure 20 the return loss is above 10 dB in the frequencies band ranging from 2.74 GHz to 13.6 GHz.

The second NB antenna, connected to Port 3, resonates at the frequencies of 7.5 GHz and 9.5 GHz (see Figure 21) which correspond to return loss values equal to 19.6 dB and 28.8 dB, respectively. Even in this case the antenna exhibits a dual-band behavior covering the frequency bands between

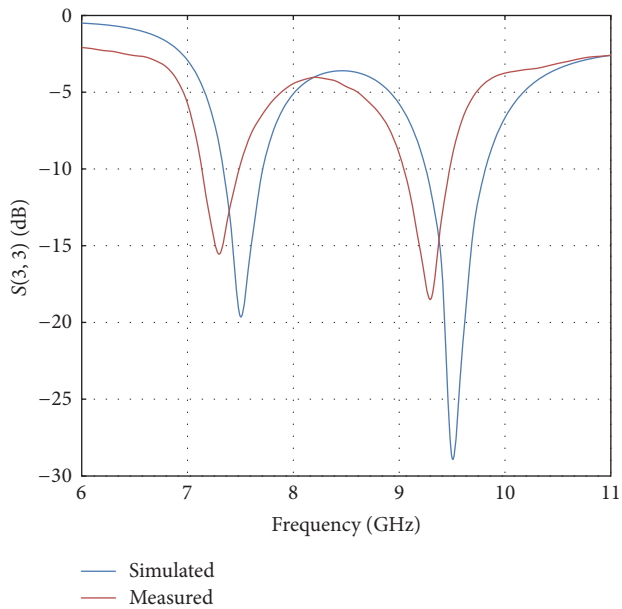

Figure 21: Comparison of simulated and measured reflection coefficients of the second NB antenna.

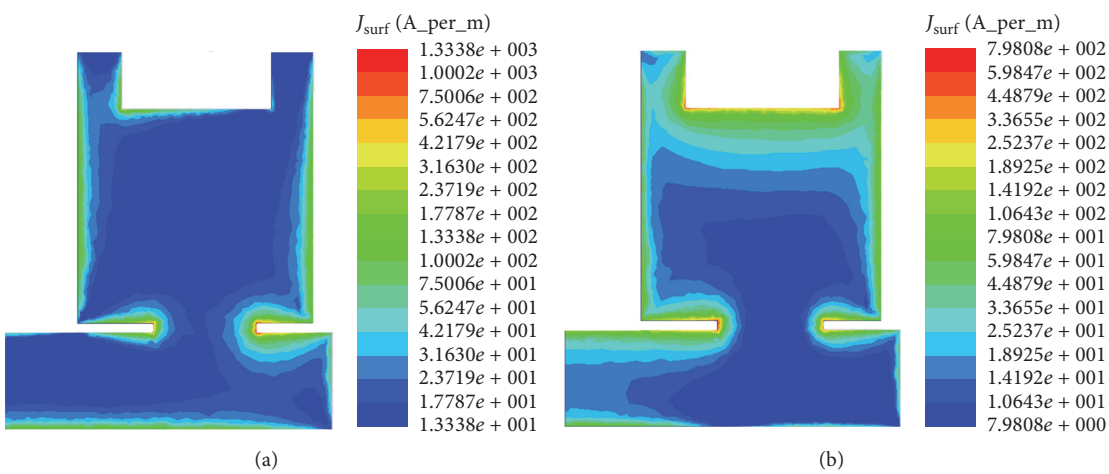

Figure 22: Simulated surface current distribution on the NB antenna at (a) 7.5 GHz and (b) 9.5 GHz.

7.33 GHz and 7.7 GHz and between 9.23 GHz and 9.82 GHz. Surface current distributions on the proposed NB antenna at 7.5 GHz and 9.5 GHz are shown in Figure 22. From Figure 22, it appears that the stub added to the microstrip line is responsible for the energy emission in the lower resonating band, while the slot realized in the rectangular patch excites the higher resonating band. From the radiation patterns in Figure 23, it appears that the antenna gains reach values of 3.64 dB and 3.2 dB, respectively. Also in this case the antenna sizing has required an accurate parametric study aimed at identifying the length of the slot and the stub used to realize a dual-band behavior. For the sake of completeness in Figure 24 the frequency behaviors of the scattering parameter S_{33} as the length of the slot and the stub increases are shown. From these curves it results that the optimized length of the slot is 1.45 mm, while that of the stub is 8.75 mm. Finally, Figure 25 shows the frequency behavior of the scattering parameter S_{13} from which the excellent electrical isolation between the UWB antenna and the second NB antenna can be noticed. All measured data clearly state that there is a good agreement between the simulated and measured results. However, there are slight shifts and changes that may be caused by fabrication faults, connector losses, improper soldering, and measurement process.

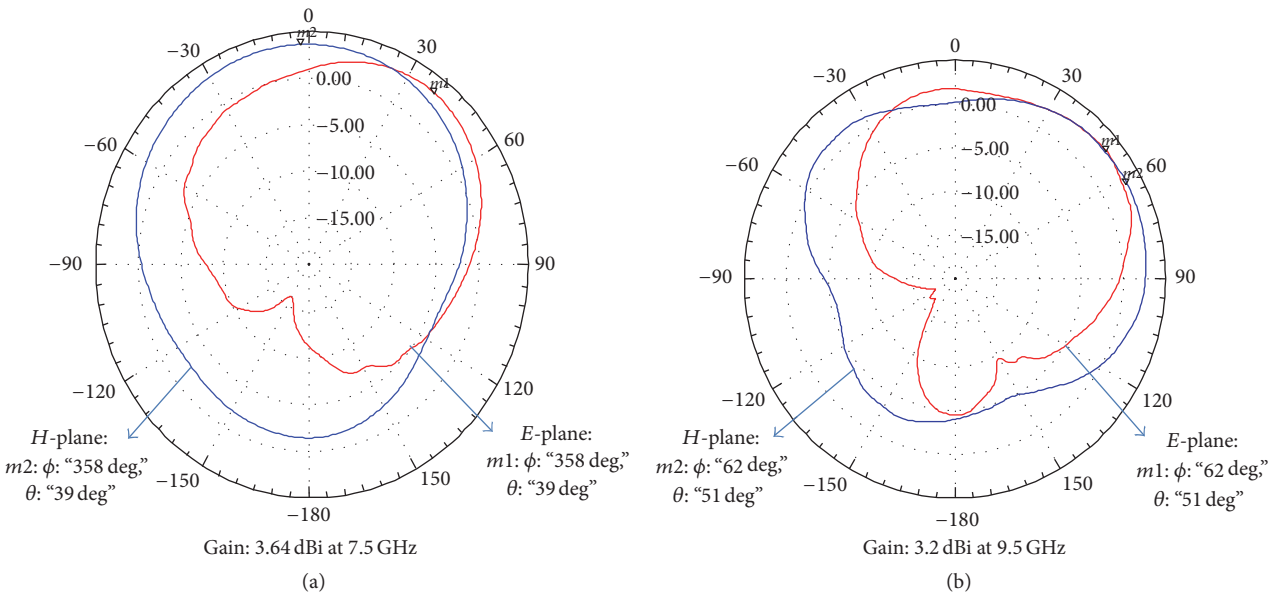

Figure 23: 2D radiation patterns of the NB antenna at (a) 7.5 GHz and (b) 9.5 GHz.

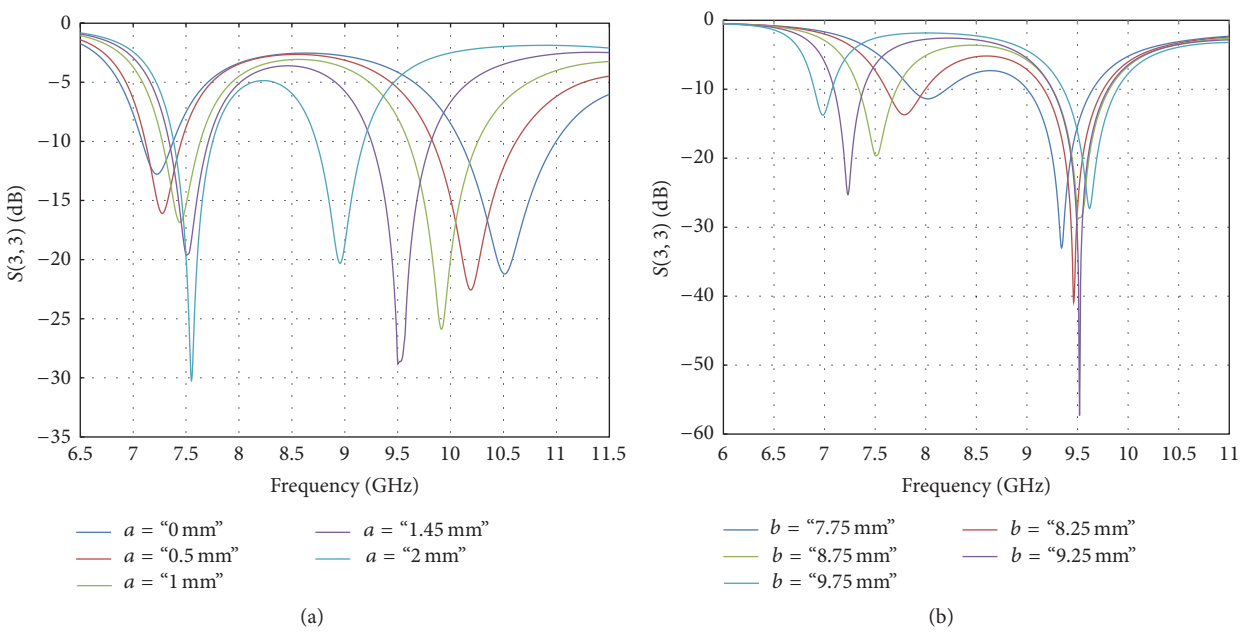

Figure 24: Reflection coefficients of the second NB antenna for (a) slot length variations and (b) microstrip stub length variations.

4. Conclusion

In this paper, an antenna system composed of three antennas integrated in the same substrate, employed for the realization of cognitive radios, has been presented. It is employed with two narrow band antennas to overcome the drawbacks of the reconfigurable antennas during their practical implementation. So, after a brief discussion concerning the characteristics of cognitive radios, purposes of the UWB antenna and of the two narrow band antennas forming the proposed antenna system have been described. Then, the analysis and design of each antenna have been illustrated in detail. A full-wave commercial software based on the FEM method has been used for an accurate prediction of the proposed antennas performances. The antenna measurements carried out on an antenna prototype have shown a good agreement with the

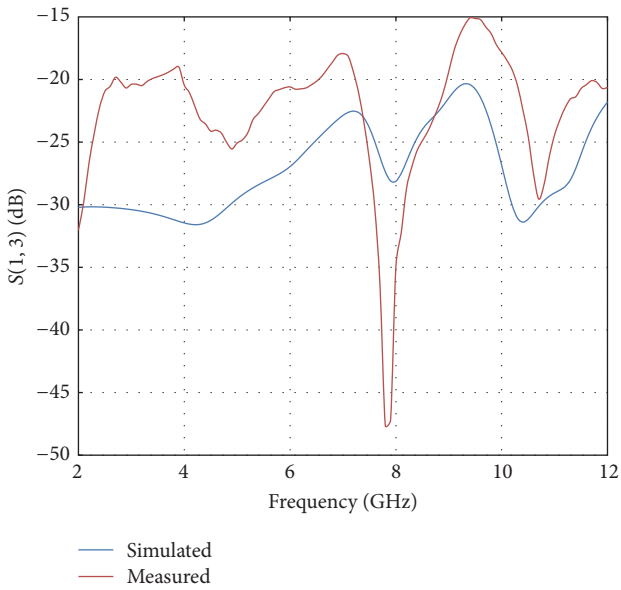

Figure 25: Comparison of simulated and measured transmission coefficients between the UWB and the second NB antenna ports.

experimental measurements. Because of compact structure and better performance, proposed system can be a good candidate for emerging cognitive radio technology.

Competing Interests

The authors declare that they have no competing interests.

References

[1] M. Al-Husseini, K. Kabalan, A. El-Hajj, and C. Christodoulou, "Cognitive radio: UWB integration and related antenna design," in *New Trends in Technologies: Control, Management, Computational Intelligence and Network Systems*, M. J. Er, Ed., INTECH, Rijeka, Croatia, 2010.

[2] Y. Tawk, M. Bkassiny, G. El-Howayek, S. K. Jayaweera, K. Avery, and C. G. Christodoulou, "Reconfigurable front-end antennas for cognitive radio applications," *IET Microwaves, Antennas and Propagation*, vol. 5, no. 8, pp. 985–992, 2011.

[3] S. K. Jayaweera and C. Mosquera, "A dynamic spectrum leasing (DSL) framework for spectrum sharing in cognitive radio networks," in *Proceedings of the 43rd Asilomar Conference on Signals, Systems and Computers*, pp. 1819–1823, Pacific Grove, Calif, USA, November 2009.

[4] A. Rajaie Raslan, *Metamaterial antennas for cognitive radio applications [thesis]*, Electronics Engineering Department, American University in Cairo School of Sciences and Engineering, 2013.

[5] N. Murtaza, R. K. Sharma, R. S. Thomä, and M. A. Hein, "Directional antennas for cognitive radio: analysis and design recommendations," *Progress in Electromagnetics Research*, vol. 140, pp. 1–30, 2013.

[6] L. Safatly, M. Bkassiny, M. Al-Husseini, and A. El-Hajj, "Cognitive radio transceivers: RF, spectrum sensing, and learning algorithms review," *International Journal of Antennas and Propagation*, vol. 2014, Article ID 548473, 21 pages, 2014.

[7] H. G. Schantz, "Three centuries of UWB antenna development," in *Proceedings of the IEEE International Conference on Ultra-Wideband (ICUWB '12)*, pp. 506–512, Syracuse, NY, USA, September 2012.

[8] Y. Tawk, J. Costantine, and C. G. Christodoulou, "A rotatable reconfigurable antenna for cognitive radio applications," in *Proceedings of the IEEE Radio and Wireless Symposium (RWS '11)*, pp. 158–161, Phoenix, Ariz, USA, January 2011.

[9] E. Ebrahimi, J. R. Kelly, and P. S. Hall, "Integrated wide-narrowband antenna for multi-standard radio," *IEEE Transactions on Antennas and Propagation*, vol. 59, no. 7, pp. 2628–2635, 2011.

[10] Y. Tawk and C. G. Christodoulou, "A new reconfigurable antenna design for cognitive radio," *IEEE Antennas and Wireless Propagation Letters*, vol. 8, pp. 1378–1381, 2009.

[11] M. Al-Husseini, A. Ramadan, K. Y. Kabalan, A. El-Hajj, Y. Tawk, and C. G. Christodoulou, "A simple dual-port antenna system for cognitive radio applications," in *Proceedings of the International Conference on High Performance Computing and Simulation (HPCS '10)*, pp. 549–552, Caen, France, June 2010.

[12] Y. Tawk, J. Costantine, S. Hemmady, G. Balakrishnan, K. Avery, and C. G. Christodoulou, "Demonstration of a cognitive radio front end using an optically pumped reconfigurable antenna system (OPRAS)," *IEEE Transactions on Antennas and Propagation*, vol. 60, no. 2, pp. 1075–1083, 2012.

[13] S.-H. Zheng, X.-Y. Liu, and M. M. Tentzeris, "A novel optically controlled reconfigurable antenna for cognitive radio systems," in *Proceedings of the IEEE Antennas and Propagation Society International Symposium (APSURSI '14)*, pp. 1246–1247, Memphis, Tenn, USA, July 2014.

[14] E. Erfani, J. Nourinia, C. Ghobadi, M. Niroo-Jazi, and T. A. Denidni, "Design and implementation of an integrated UWB/reconfigurable-slot antenna for cognitive radio applications," *IEEE Antennas and Wireless Propagation Letters*, vol. 11, pp. 77–80, 2012.

[15] Y. Li, W. Li, and R. Mittra, "Integrated dual-purpose narrow/ultra-wide band antenna for cognitive radio applications," in *Proceedings of the IEEE International Symposium on Antennas and Propagation and USNC-URSI National Radio Science Meeting (APSURSI '12)*, Chicago, Ill, USA, July 2012.

[16] C. G. Christodoulou, Y. Tawk, S. A. Lane, and S. R. Erwin, "Reconfigurable antennas for wireless and space applications," *Proceedings of the IEEE*, vol. 100, no. 7, pp. 2250–2261, 2012.

[17] M. Al-Husseini, A. El-Hajj, and K. Y. Kabalan, "A 1.9–13.5 GHz low-cost microstrip antenna," in *Proceedings of the IEEE International Wireless Communications and Mobile Computing Conference (IWCMC '08)*, pp. 1023–1025, Crete, Greece, August 2008.

[18] M. Al-Husseini, Y. Tawk, A. El-Hajj, and K. Y. Kabalan, "A low-cost microstrip antenna for 3G/WLAN/WiMAX and UWB applications," in *Proceedings of the International Conference on Advances in Computational Tools for Engineering Applications (ACTEA '09)*, pp. 68–70, Zouk Mosbeh, Lebanon, July 2009.

[19] N. A. Kumar and A. S. Gandhi, "Small size planar monopole antenna for high speed UWB applications," in *Proceedings of the 22nd National Conference on Communication (NCC '16)*, pp. 1–5, Guwahati, India, March 2016.

[20] M. Al-Husseini, A. Ramadan, Y. Tawk, A. El-Hajj, and K. Y. Kabalan, "Design and ground plane optimization of a CPW-fed ultra-wideband antenna," *Turkish Journal of Electrical Engineering and Computer Sciences*, vol. 19, no. 2, pp. 243–250, 2011.

[21] S. R. Zahran, O. H. El Sayed Ahmed, A. T. El-Shalakany, S. S. Saleh, and M. A. Abdalla, "Ultra wide band antenna with enhancement efficiency for high speed communications," in *Proceedings of the 31st National Radio Science Conference (NRSC '14)*, pp. 65–72, Cairo, Egypt, April 2014.

[22] G. M. Dandime and V. G. Kasabegoudar, "A slotted circular monopole antenna for wireless applications," *International Journal of Wireless Communications and Mobile Computing*, vol. 2, no. 2, pp. 30–34, 2014.

[23] K. P. Ray, "Design aspects of printed monopole antennas for ultra-wide band applications," *International Journal of Antennas and Propagation*, vol. 2008, Article ID 713858, 8 pages, 2008.

[24] FCC 1st Report and Order on Ultra-Wideband Technology, February 2002.